Multiphysics Simulation of the Effect of Sensing and Spacer Layers on SAW Velocity

Peng Zheng[*1,4], David W. Greve[2,4], and Irving J. Oppenheim[3,4]
[1]Department of Physics, Carnegie Mellon University, Pittsburgh, PA, USA
[2]Department of Electrical and Computer Engineering, Carnegie Mellon University, Pittsburgh, PA, USA
[3]Department of Civil and Environmental Engineering, Carnegie Mellon University, Pittsburgh, PA, USA
[4]National Energy Technology Laboratory, Pittsburgh, PA, USA
*5000 Forbes Ave. Pittsburgh, PA 15213, USA, Email: pengzhen@andrew.cmu.edu

Abstract: Surface acoustic wave gas sensors use a chemically sensitive resistive layer to detect gas concentration. The resistivity of the sensing material, the sensing layer thickness, and the spacer layer thickness all affect the surface wave propagation velocity. Existing analytic theory relates the change in velocity to various parameters. However some variables in this theory (such as the effective permittivity) are not unambiguously defined. Accurate simulations require inclusion of electrostatic effect and acoustic wave propagation in the sensing layer and spacer layer. In this paper we performed simulation of surface acoustic wave propagation in layered structure using multiphysics finite element package COMSOL 3.4a and 3.5, 2D piezo plane strain mode. The effect of thickness and materials of sensing and spacer layer are analyzed to optimize SAW gas sensor design.

Keywords: Surface Acoustic Wave, Layered Structure, Gas Sensor, Sensitivity, ZnO, Si_3N_4, SiO_2, $LiNbO_3$

1. Introduction

Surface acoustic waves (SAW) are acoustic waves traveling along the surface of an elastic body, with an amplitude decays exponentially with depth into the bulk of the body [1]. SAW devices typically use an interdigitated transducer (IDT), consisting of thin metal electrode with equal spacing and width, to generate and receive surface acoustic waves in piezoelectric materials [2]. SAW devices can be used as a sensor by the detection of the surface acoustic wave velocity change, caused by perturbations to the piezoelectric substrate surface. Various types of sensors, based on the changes of the surface conductivity [3-6], mass [7-10], strain [11], and temperature [12] have been explored. Conductivity based SAW sensors are particularly promising for gas sensing in hostile environments, such as the exhaust of oxy-fuel coal combustors. In this application, exhaust gas sensors make it possible to control the combustion process so as to achieve a nearly pure carbon dioxide exhaust suitable for geologic sequestration.

Perturbation theory has been widely used in the analysis of surface acoustic wave propagation in the conductivity based gas sensors [1]. However, in the layered structures increasingly used in sensor design, the perturbation analysis is too complex. In addition accurate simulations require inclusion of both the electrostatic effect and the elastic wave propagation in the sensing and spacer layers, which is not considered in perturbation theory. Therefore accurately multiphysics finite element simulation is needed to analyze the conductivity based SAW sensor. In this paper, surface acoustic wave propagation in the commonly used $ZnO/Si_3N_4/LiNbO_3$ and $ZnO/SiO_2/LiNbO_3$ layered structures is simulated using COMSOL 3.4a. The effect of thickness and composition of the sensing and spacer layer are analyzed. The simulation results are valuable for design of SAW sensors for the oxygen sensing application.

2. Conductivity Based SAW Gas Sensor

When a surface acoustic wave propagates in a piezoelectric material, a layer of bound charges are generated at the surface. The electrical field generated by the bound charge creates a force that opposes the mechanical deformation. This is equivalent to a mechanical stiffness increase, called piezoelectric stiffening. When a conducting film is deposited on top of the piezoelectric material, the electrical boundary

condition is changed from that of a free surface to a short circuit in the limit of infinite conductivity. Charge carriers in the conducting film can then quickly redistribute to generate an electrical field to compensate the electrical field of the bound charge. The result of adding a conductive film is then a release of the piezoelectric stiffening and a decrease of the surface acoustic wave velocity. This phenomenon is called the electro-acoustic effect, and is directly related to the electromechanical coupling coefficient K^2 [1], where

$$K^2 = -2\frac{\Delta v}{v_f} \qquad (1)$$

v_f is the phase velocity at a free surface and Δv is the velocity change caused by the conducting layer.

In the conductivity based SAW gas sensor, a resistive chemically sensitive layer is deposited on the piezoelectric substrate surface. The interaction of gas molecules with the sensing layer changes the sheet conductivity and perturbs the electrical boundary condition. As a result, the surface acoustic wave velocity is changed by the interactions between gas and sensing layer. The relation between conductivity of sensing layer and surface acoustic wave velocity can be derived by the perturbation theory

$$\frac{\Delta v}{v_f} = \frac{-K^2}{2}\frac{1}{1+\left(\frac{v_f \varepsilon_p(k_0)}{\sigma_0 t}\right)^2} \qquad (2)$$

where $\varepsilon_p(k_0)$ is the effective permittivity in the absence of the piezoelectric effect, k_0 is the wavenumber of the surface acoustic wave, σ_0 is the bulk conductivity of the sensing layer, and t is the sensing layer thickness. The SAW sensor sensitivity S can be determined by taking derivative of Eq. 2 with respect to the sensing layer conductivity σ_0

$$S = -\frac{d(\Delta v/v_f)}{d\sigma_0} = \frac{K^2 v_f^2 \varepsilon_p(k_0)^2}{\left(1+\frac{v_f^2 \varepsilon_p(k_0)^2}{\sigma_0^2 t^2}\right)^2 \sigma_0^3 t^2} \qquad (3)$$

Fig.1 shows an example of calculated surface acoustic wave velocity changes and sensor sensitivity as a function of the conductivity of a 100 nm thick resistive sensing layer with YZ cut $LiNbO_3$ as substrate. From the equation and Fig.1, we can see that the peak in sensitivity occurs when

$$\sigma_c = 0.58 v_f \varepsilon_p(k_0)/t \qquad (4)$$

To get the best sensor efficiency, the conductivity of sensing layer must fall in the range around σ_c . The maximum sensor sensitivity S_c can be derived by taking Eq. 4 into Eq. 3

$$S_c = 0.325\frac{K^2 t}{v_f \varepsilon_p(k_0)} \qquad (5)$$

In general we want the maximum sensor sensitivity Sc to be as large as possible. From the expression for Sc, we can see that the sensor sensitivity is determined by effective permittivity $\varepsilon(k_0)$, surface acoustic wave velocity v_0 , electromechanical coefficient K^2 , and sensing layer thickness t. However, in the layered structures $ZnO/Si_3N_4/LiNbO_3$ and $ZnO/SiO_2/LiNbO_3$, $\varepsilon(k_0)$ and K^2 are not unambiguously defined. Furthermore the mechanical effect of the sensing and spacer layers are not included in the analytical model. We will therefore use of finite element simulations to obtain accurate predictions of the SAW sensor sensitivity.

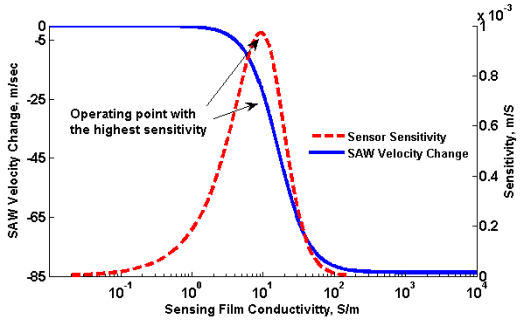

Figure 1 Calculated surface acoustic wave velocity changes (solid blue line) and sensor resistivity (red dashed line) as a function of sensing layer conductivity. Substrate is YZ $LiNbO_3$. The thickness of sensing layer is 100 nm. Calculation is based on the parameter in Ref [1]

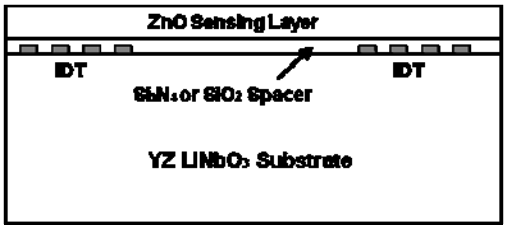

Figure 2 Schematic of proposed layered SAW sensor

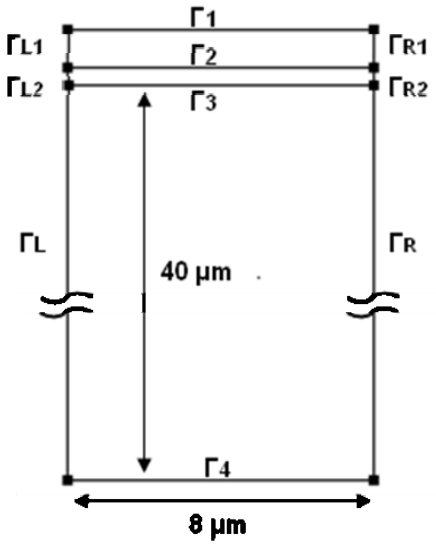

Figure 3 Geometry employed in the simulation.

3. Multiphysics Simulation of Surface Acoustic Wave Layered Structure

Fig. 2 shows the schematic of a layered SAW sensor. ZnO is used as the chemically resistive sensing layer. Si_3N_4 or SiO_2 are two candidates for the spacer to isolate the IDTs from the sensing layer. YZ-cut $LiNbO_3$ is used as piezoelectric substrate. Rayleigh surface acoustic waves with 8 μm wavelength are excited by the IDT. The spacer composition and the spacer and sensing layer thicknesses all influence the sensitivity.

We use the multiphysics finite element package COMSOL 3,4a and 3.5, 2D piezo plane strain mode (smppn) to simulate the surface acoustic wave propagation in the layered structure (Fig. 3). This application mode assumes that the out of plane strain is zero. This is a valid assumption since the Rayleigh waves have no displacement in the out of plane direction. To further simplify the simulation, periodic boundary conditions are used. The periodic boundary conditions set the right (Γ_R, Γ_{R1}, Γ_{R2}) and the left (Γ_L, Γ_{L1}, Γ_{L2}) vertical boundary to have the same displacement and potential. This implies that simulated surface acoustic wave wavelength will be an integral fraction of the width of the simulation domain which is 8 μm. Eigenfrequency analysis of the 2D layered structure is then performed to simulate the surface acoustic wave propagation. In the solver parameters settings, an estimated eigenfrequency need to be provided before simulation so that COMSOL could search for solutions around the estimated eigenfrequency. There are many solutions that are not surface acoustic wave, for example bulk acoustic wave launched from top. The surface acoustic wave wavelength is equal to the width of simulation domain 8 μm at the lowest eigenfrequency with a surface acoustic wave characteristic. The surface acoustic wave phase velocity can be calculated by multiplying the eigenfrequency by the 8 μm wavelength.

The 2D layered structure simulated has 40 μm thick Y-Z cut $LiNbO_3$ as the substrate, a Si_3N_4 or SiO_2 spacer layer and a top ZnO resistive sensing layer. The depth of the $LiNbO_3$ substrate is 5 wavelengths to limit the size of the simulation. Vacuum or air could be simulated above the sensing layer, but is not considered here because all the materials used here have relatively high permittivity.

The $LiNbO_3$ substrate is solved by the following governing equation as piezoelectric materials

$$\mathbf{T} = c_E \mathbf{S} - e^T \mathbf{E} \quad (6)$$

$$\mathbf{D} = e\mathbf{S} + \varepsilon_S \mathbf{E} \quad (7)$$

Where **T** is the stress tensor, **S** is the strain tensor, **D** is the electric displacement vector, **E** is the electric field vector, c_E , e and ε_S are elastic, piezoelectric and dielectric matrix respectively. The spacer layer and sensing layer are solved in the decoupled, isotropic materials mode with electrical equation enabled. In COMSOL 3.4a both of the elastic equation and electrostatic equation are solved under this materials mode as following

$$\mathbf{T} = c_E \mathbf{S} \quad (8)$$

$$-\nabla \cdot (\varepsilon_0 \varepsilon_r \nabla V) = \rho_v \quad (9)$$

where w is the egenfrequency, ε_0 is the electrical permittivity of the free surface, ε_r is the relative electrical permittivity of the materials, V is the potential, ρ_v is the volume charge density. Alternatively one can also perform a multiphysics simulation combining 2D plane stain mode (smpn) and 2D electrostatic mode (emes) in the spacer and sensing layer, where the same equations, Eq. 8 and Eq. 9, are solved as in the decoupled, isotropic materials mode in 2D piezo strain simulation.

A complex dielectric permittivity $\varepsilon_r + j\sigma/\omega\varepsilon_0$ is introduced to simulate the effect of a layer of

conductivity σ at frequency ω. Eq. 9 is then transformed into

$$-\nabla\cdot((\frac{\sigma}{jw}+\varepsilon_0\varepsilon_r)\nabla V)=\rho_v \qquad (10)$$

In COMSOL 3.5, Eq. 9 is replaced by Eq. 10 in the decoupled, isotropic materials mode, where conductivity can be directly input in the subdomain setting. From the equation above, we can see that both of the electrical and mechanical effect of spacer and sensing layer are considered in the simulation.

Boundary conditions (BC) of the simulation are listed in table 1. Materials constant are listed in Appendix.

	Mechanical BC	Electrical BC
Γ_1	Free	zero charge /symmetry
Γ_2, Γ_2	Free	Continuity
Γ_4	Fixed	Ground
Γ_R, Γ_{R1}, Γ_{R2} Γ_L, Γ_{L1}, Γ_{L2}	Periodical boundary condition	

Table 1 Boundary condition of simulation

4. Results and Discussion

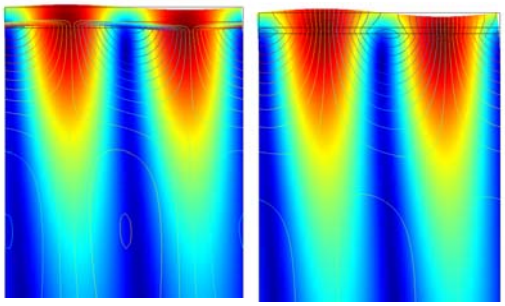

Figure 4 Simulation result of layered structure $ZnO/Si_3N_4/LiNbO_3$. Picture on the left: conducting sensing layer; picture on the right: insulating sensing layer. The color shows the displacement strength; the contour curve shows the electrical potential.

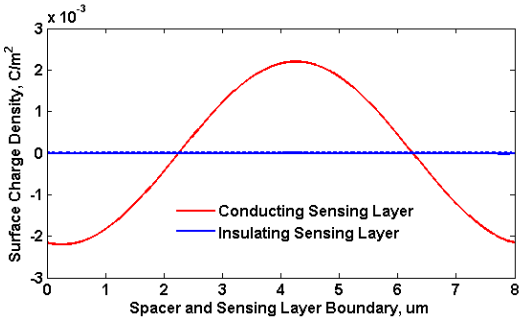

Figure 5 Surface charge density on spacer and sensing layer boundary Γ_2

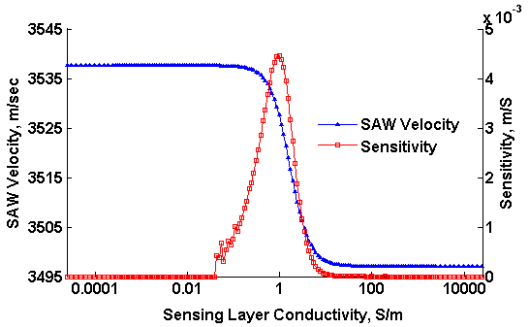

Figure 6 Surface acoustic wave velocity and sensitivity of a $ZnO/Si_3N_4/LiNbO_3$ layered structure based on simulation result. ZnO thickness is 600 nm. Si_3N_4 thickness is 300 nm.

A series of simulations of surface acoustic wave propagation were performed in different layered structures with varying conductivity in the sensing layer to simulate the effect of gas sensing. The sensitivity of each layered structure is also calculated using Eq. 3 based on the simulation result. Fig. 4 and Fig. 5 shows a comparison of the simulation result ranging from insulating ($\sigma_0 = 0$) to conducting ($\sigma_0 = \infty$) sensing film. In the simulation result with conducting sensing film, charge density on the sensing layer and spacer boundary varies along the interface, while in the result with insulating sensing film the charge density is almost zero along the sensing layer and spacer boundary (Fig. 5). In addition we can see that electrical field does not penetrate into the conducting sensing layer from the electrical contour curve (Fig. 4). This indicates that charge carriers in the conducting sensing layer and spacer boundary redistribute to oppose penetration of the external electrical field. As a result the electrical field generated by the bound charge in the piezoelectric substrate surface is compensated by the electrical field produced by the charge in the conducting sensing film, which then cause the the release of piezoelectric stiffening and surface acoustic wave velocity decrease. Fig. 6 shows the simulation result of surface acoustic wave velocity and sensitivity as a function of sensing layer conductivity in a $ZnO/Si_3N_4/LiNbO_3$ layered structure. It shows the similar structure as the calculated result in Fig. 1.

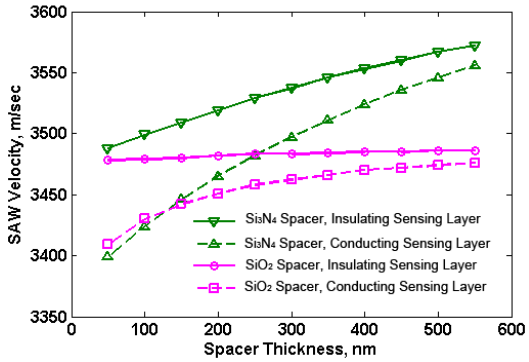

Figure 7 Surface acoustic wave velocity with conducting and insulating sensing film in layered structure $ZnO/Si_3N_4/LiNbO_3$ and $ZnO/SiO_2/LiNbO_3$ with different spacer thickness

Fig. 7 shows the surface acoustic wave speed of conducting sensing and insulating sensing layer in the $ZnO/Si_3N_4/LiNbO_3$ and $ZnO/SiO_2/LiNbO_3$ layered structures with different spacer thickness. We can see that structure with insulating sensing layers always have larger surface acoustic wave velocity than those with conducting sensing layer in the same structure, which is the result of reduced electro-acoustic effect. We can also see that surface acoustic wave velocity increases as the spacer thickness increases. In addition surface acoustic wave velocity of structures with Si_3N_4 as spacer increase more than those with SiO_2 as spacer. This is because Si_3N_4 has larger acoustic wave speed than SiO_2.

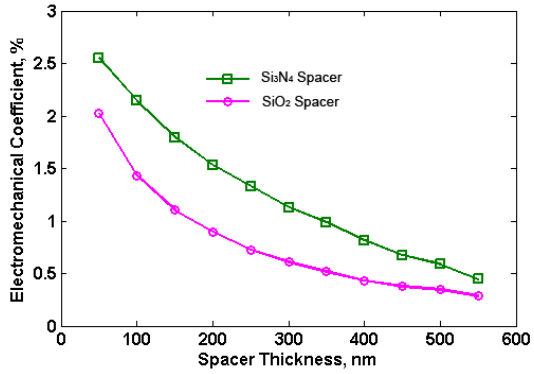

Figure 8 Electromechanical coefficients of $ZnO/Si_3N_4/LiNbO_3$ and $ZnO/SiO_2/LiNbO_3$ layered structures with different spacer thickness

Fig. 8 shows the electromechanical coefficient (calculated from Eq. 1) of the layered structure with varying spacer thickness, where $ZnO/Si_3N_4/LiNbO_3$ layered shows larger electromechanical coupling than $ZnO/SiO_2/LiNbO_3$. However from Eq. 5 we can see that this does not necessarily mean $ZnO/Si_3N_4/LiNbO_3$ has a better sensitivity than $ZnO/SiO_2/LiNbO_3$ structure.

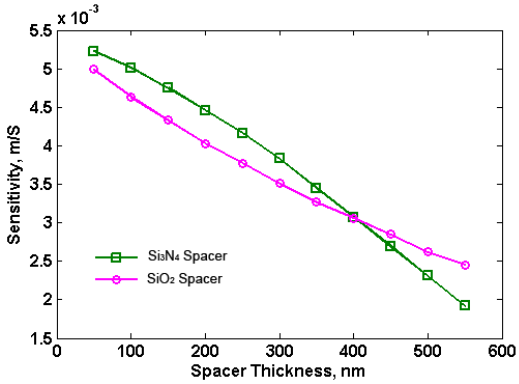

Figure 9 The maximum sensitivity of $ZnO/Si_3N_4/LiNbO_3$ and $ZnO/SiO_2/LiNbO_3$ layered structures with different spacer thickness

Fig. 9 shows the maximum sensitivity of $ZnO/Si_3N_4/LiNbO_3$ and $ZnO/SiO_2/LiNbO_3$ layered structures based on the simulation result. It shows that the maximum sensitivity decreases as the spacer thickness increases. This is because increasing separation of the sensing layer from the substrate reduces the influence of a change of conductivity on the electric field. The $ZnO/Si_3N_4/LiNbO_3$ structure has better sensitivity than $ZnO/Si_3N_4/LiNbO_3$ when the spacer is thinner than 400 nm. These results mean that the thickness of spacer should be as small as possible to get the best sensitivity. When the spacer is thinner than 400 nm, Si_3N_4 spacer is the best choice for the layered structure. For our SAW gas sensor application, spacer thickness is below 400 nm. Therefore Si_3N_4 spacer is the better selection and used in the following simulation.

Surface acoustic wave propagation with varying ZnO sensing layer thickness are simulated in $ZnO/Si_3N_4/LiNbO_3$ structure. The Si_3N_4 spacer thickness is set to be 100 nm, 200 nm, and 300 nm. The ZnO sensing layer thickness varies from 100 nm to 1000 nm. Fig. 10 shows the surface acoustic wave velocity of layered structure with conducting or insulating sensing layer. It shows that surface acoustic

wave velocity decreases slightly when the sensing layer thickness increases.

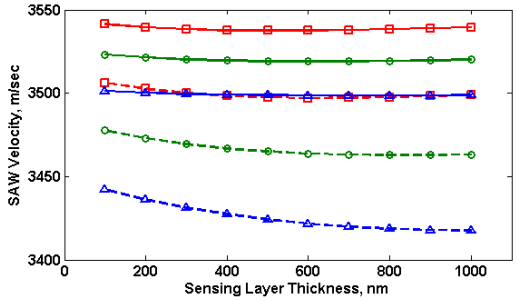

Figure 10 Simulated surface acoustic wave velocity in layered structure $ZnO/Si_3N_4/LiNbO_3$ with different spacer and sensing layer thickness. The red solid curve: 300 nm spacer and insulating sensing layer; red dashed curve: 300 nm spacer and conducting sensing layer; green solid curve: 200 nm spacer and insulating sensing layer; green dashed curve: 200 nm spacer and conducting sensing layer; blue solid curve: 100 nm spacer and insulating sensing layer; blue dashed curve: 100 nm spacer and conducting sensing layer.

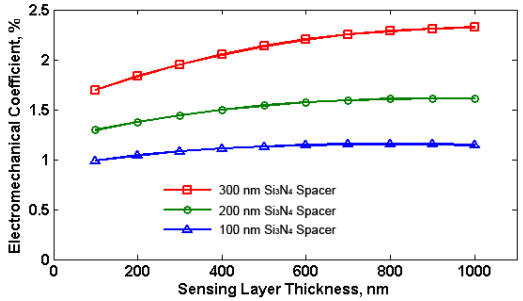

Figure 11 Electromechanical coefficients of $ZnO/Si_3N_4/LiNbO_3$ layered structures with different spacer and sensing layer thickness

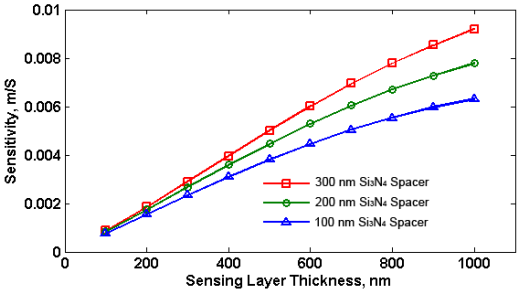

Figure 12 The maximum sensitivity of $ZnO/Si_3N_4/LiNbO_3$ and layered structures with different spacer and sensing layer thickness

Fig. 11 shows the electromechanical coefficient of these structures. It shows a small increase of electromechanical coupling coefficient as the sensing layer thickness increase.

Fig. 12 shows the maximum sensitivity of these structures. It shows that the maximum sensitivity increases almost linearly with the sensing layer thickness. This agrees with the theoretical calculation from Eq. 5 where the maximum sensitivity is proportional to the sensing layer thickness. From these simulation results we can see that a thick sensing layer is preferred in the sensor design. However, thick sensing layer may degrade the sensor response time due to the slower diffusion in the sensing layer.

7. Conclusions

In this paper we simulated surface acoustic wave propagation in $ZnO/Si_3N_4/LiNbO_3$ and $ZnO/SiO_2/LiNbO_3$ layered structures using multiphysics finite element package COMSOL 3.4a, 2D piezo plane strain mode. From the eigenfrequency corresponding to a surface acoustic wave, we determined the resulting velocity. Sensor sensitivity is calculated based on the simulation result to optimize SAW sensor design. The effect of thickness and materials of sensing and spacer layer on the sensitivity are analyzed. The simulation results show that the maximum sensitivity increase as the spacer gets thinner or the sensing layer gets thicker. In addition the $ZnO/Si_3N_4/LiNbO_3$ layered structure shows higher sensitivity than the $ZnO/SiO_2/LiNbO_3$ layered structure with a spacer thickness ranges from 50 nm to 400 nm. For spacer thickness over 400 nm, $ZnO/SiO_2/LiNbO_3$ structure has higher sensitivity than $ZnO/Si_3N_4/LiNbO_3$ structure. For our application where spacer thickness is below 400 nm, $ZnO/Si_3N_4/LiNbO_3$ is the better selection for SAW gas sensor design.

8. References

1. D. S. Jr Ballantine et al. , *Acoustic Wave Sensors - Theory, Design, and Physico-Chemical Applications*, 36-89. Elsevier (1997)
2. White, R. M. Surface elastic waves, *Proc. IEEE*, **58**, 1238-1276 (1970)
3. A. J. Ricco, S. J. Martin, and T. E. Zipperian, Surface acoustic wave gas sensor based on film conductivity changes, *Sensors and Actuators*, **Vol. 8**, 319-333 (1985)

4. M.S. Nieuwenhuizen and A.J. Nederlof, A silicon-based SAW chemical sensor for NO2 by applying a silicon nitride passivation layer, *Sensors and Actuators B: Chemical*, **Vol. 9**, 171-176 (1992)
5. S.J. Ippolito, et al. , Layered WO_3/ZnO/36◦ $LiTaO_3$ SAW gas sensor sensitive towards ethanol vapour and humidity, *Sensors and Actuators B*, **Vol. 117**, 442–450 (2006)
6. Wieslaw P. Jakubik and Marian W. Urbanczyk,, SAW hydrogen sensor with a bilayer structure based on interaction speed, *Sensors and Actuators B,* **Vol. 106**, 602-608 (2005)
7. J. Du, et al. , A study of Love wave acoustic sensors, *Sensors and Actuators A: Physical*, **Vol. 55**, 211-219 (1996)
8. B. Jakoby, et al. A novel molecularly imprinted thin lm applied to a love wave gas sensor, *Sensors and Actuators A: Physical*, **Vol. 76**, 93-97 (1999)
9. C. Zimmermann, et al., A love wave gas sensor coated with functionalized polysiloxane for sensing organophosphorus compounds, *Sensors and Actuators B: Chemical*, **Vol. 76**, 86-94 (2001)
10. M. Penza, F. Antolini, and M. Vittori-Antisari, Carbon nanotubes as SAW chemical sensors materials, *Sensors and Actuators B: Chemical*, **Vol. 100**, 47-59 (2004)
11. Vasundara V Varadan, et al. , Wireless passive IDT strain microsensor, *Smart Materials and Structures*, **Vol. 6**, 745-751 (1997)
12. X. Q. Bao, W. Burkhard, V. V. Varadan and V. K. Varadan, SAW Temperature Sensor and Remote Reading System, *Proceeding of the IEEE International Symposium on Ultrasonics*, 583-585 (1987)

9. Acknowledgements

This work was performed in support of ongoing research in sensor systems and diagnostics at the National Energy Technology Laboratory under RDS contract DE-AC26-04NT41817. This technology is being explored as a sensor to evaluate oxygen levels in advanced oxy-fuel powerplants that can capture CO_2.

10. Appendix

Materials constant

$LiNbO_3$
Density $\rho = 4647$ kg/m^3
Elastic Matrix $\mathbf{c_E}$

$$\mathbf{c_E} = \begin{pmatrix} 2.424 & 0.752 & 0.752 & 0 & 0 & 0 \\ 0.752 & 2.03 & 0.573 & 0 & 0.085 & 0 \\ 0.752 & 0.573 & 2.03 & 0 & -0.085 & 0 \\ 0 & 0 & 0 & 0.752 & 0 & 0.085 \\ 0 & 0.085 & -0.085 & 0 & 0.595 & 0 \\ 0 & 0 & 0 & 0.085 & 0 & 0.595 \end{pmatrix} \times 10^{11} [\text{Pa}]$$

Coupling matrix e

$$\mathbf{e} = \begin{pmatrix} 1.33 & 0.23 & 0.23 & 0 & 0 & 0 \\ 0 & 0 & 0 & -2.5 & 0 & 3.7 \\ 0 & -2.5 & 2.5 & 0 & 3.7 & 0 \end{pmatrix} [\text{C/m}^2]$$

Relative permittivity $\boldsymbol{\varepsilon_{rs}}$

$$\boldsymbol{\varepsilon_{rs}} = \begin{pmatrix} 28.7 & 0 & 0 \\ 0 & 85.2 & 0 \\ 0 & 0 & 85.2 \end{pmatrix}$$

Si_3N_4
Yougn's modulus E = 250 ×10^9 Pa
Poisson's ratio $v = 0.23$
Density $\rho = 3100$ kg/m^3
Relative permittivity $\varepsilon_r = 9.7$

SiO_2
Yougn's modulus E = 70 ×10^9 Pa
Poisson's ratio $v = 0.17$
Density $\rho = 2200$ kg/m^3
Relative permittivity $\varepsilon_r = 4.2$

ZnO
Yougn's modulus E = 210 ×10^9 Pa
Poisson's ratio $v = 0.33$
Density $\rho = 5676$ kg/m^3
Relative permittivity $\varepsilon_r = 8.3$